The International Journal of Advanced Manufacturing Technology
https://doi.org/10.1007/s00170-024-13640-6

ORIGINAL ARTICLE

Investigation of the transient change of the cutting force during the milling of C45 and X5CrNi18-10 steel taking into account the dynamics of the electro-mechanical measuring system

Zoltán Pálmai[1] · János Kundrák[1] · Csaba Felhő[1] · Tamás Makkai[1]

Received: 18 December 2023 / Accepted: 12 April 2024

Abstract
The possible methods of determining the cutting force—due to the great practical importance of knowing the force—have long been and are still intensively studied areas of cutting theory. In milling, cutting is a series of successive short material removals. During force measurement in such cases, the transient process that can be detected at the beginning of the process can influence the nature of the entire cutting cycle. The present study reports on the research, the aim of which was to explore the dynamic process of cutting force measurement in intermittent cutting. The measurements were made during face milling of C-steel and highly alloyed steel (X5CrNi 18–10). The milling head contained a single insert, with which the disturbing interaction of the multiple cutting edges was eliminated. As a result of the work, a method suitable for examining the close relationship between the initial transient nature of the milling cycle and the decay, as well as a mathematical model for the decay process, was developed. The model was validated with cutting experiments and measurements. The achieved results can be used to better understand the process of chip removal and to determine the actual power requirements of milling works.

Keywords Cutting · Milling · Transient force · Mathematical transient model

1 Introduction

Cutting is one of the most important technologies in the machine industry, despite the fact that it can also be considered one of the oldest processes. Its theory was also developed a long time ago; Finnie [1] reviewed the development of the previous hundred years nearly seven decades ago. Examining the theory of chip formation, Bayard [2] listed 48 models in his thesis that sought to describe the plasticity-theoretical and thermomechanical laws of this technology.

Knowing the cutting force is necessary and useful for several phases of the production operations. The measurement of cutting force is increasingly used to monitor tool wear [3, 4]. Meanwhile, in some cases, it is not only necessary to know the cutting force, but also its fluctuation. For example, Li, Z., and G. Wang [5] have detected force fluctuations during milling, and they have deduced the tool wear from that. Chuangwen et al. [6] also investigated the relationship between cutting force and vibrations in stainless steel milling, and collected data on the stability of the machining process. Research into the relationship between vibration and cutting forces leads to more and more new results. This is also evident in the review by Navarro-Devia et al. [7]. Twenty-five percent of the processed studies deal with the application of cutting forces.

The need to know the cutting force arises in many different areas of technology. Tomicek and Molotovnik [8], for example, studied the relationship between cutting force and tool wear during profile milling of Inconel 738LC material,

Highlights
1. The initial phase of the $F(t)$ curve detected during the measurement of the cutting force and the phase of decay following chip removal are transient.
2. The two curves can be superimposed by mirroring them, so the initial transient character is determined by the decay of the measurement system.
3. A mathematical model was created for the decay process based on the analogy of a circuit connected in series.
4. The data measured during the milling of C45 and X5CrNi18-10 steel proved the correctness of the model.
5. In the model, the specific energy requirement can be calculated using the law of conservation of momentum.

✉ János Kundrák
janos.kundrak@uni-miskolc.hu

[1] Institute of Manufacturing Science, University of Miskolc, 3515 Miskolc, Egyetemváros, Hungary

Published online: 11 May 2024

and based on this, they were able to provide useful information for practical technology. Pan et al. [9] has considered the recrystallization effects for force modelling of Inconel 718 laser-assisted end milling. As shown by Chunlei Song [10], knowing the cutting force is also useful for predicting the milling stability. Cekic et al. [11] measured the cutting force during high-speed face milling of hardened alloy steel. They found that at super-high cutting speeds, the detected cutting force decreases. A similar finding was made by Biró et al. [12]. These are in line with the well-known statement made by Salomon [13], that this is also observed in the measured values of the cutting temperature in the case of a higher cutting speed.

These application examples also show that knowledge of the cutting force is necessary and useful from several points of view. Therefore, one of the main goals of the researchers of cutting theory has long been to determine the force required for chip removal. Regarding the empirical power functions that were used for decades to calculate the cutting force [14], it was more and more often found that the values calculated with them often differed strongly from the measured data.

Meanwhile, the application of the finite element method (FEM), another direction of chip formation research, also developed rapidly. At first, the FEM was considered a phenomenological method, which made it possible to calculate the stress in the chip root, the resulting deformation, deformation velocity, and temperature using empirical data. This makes it necessary to meet particularly complicated requirements under the intensively changing conditions of intermittent cutting. The key to the method is the use of a constitutive equation that is suitable for characterizing the real metal-physical processes that occur in the chip root. However, because of this, the accuracy of predictions from FEM-based cutting models has been a constant problem. Material models are often fitted to base data that do not represent the extreme deformation and thermodynamic conditions experienced during cutting. This is especially complicated for intermittent chip removal, such as milling. And since this technology is widely used by industry due to its high productivity, this special method of material formation is widely and intensively researched even today.

The attention of researchers has therefore increasingly turned to the microstructure of machined metals and chips. Solutions closer to reality were sought with the tools of solid body physics. Turkovich's [15] research on dislocation theory was already able to rely on valuable previous research results. These were confirmed by the transmission, electron, and scanning microscope investigations by Black and Ramalingam [16–19]. In the metallurgical research related to these laboratory tests—as shown by Li et al. [20]—the metal deformation, which is basically the formation of determining dislocations, can be characterized with a nanosecond time scale. Even under these extreme conditions, more and more results have been obtained that are of concrete use in constitutive equations. Of particular interest from the cutting perspective, Li et al. [21] found a strict correlation between the movement of different high-speed dislocations. Melcote et al. [22] presented a physically based constitutive model that proved the relationship between the grain refinement process and chip formation in the shear band. Rodriguez et al. [23] developed a metallurgically based constitutive finite element model describing the behavior of the particles to investigate the problems of complex large deformation configurations. Xu et al. [24] showed that the dynamic recrystallization occurring in the material can be effectively modelled during high-speed machining of Ti6Al4V alloy.

The research results of Bai and Zhen Tong [25], which were obtained during high-performance cutting of AISI 4140 steel, are particularly noteworthy from the point of view of the study of the deformation processes taking place during milling. They showed that at the beginning of the machining of a specific section, the mechanical stresses calculated by the FEM method they developed do not increase abruptly, rather, they grow steeply but gradually. This transient process has been found to take 1–3 ms. Pálmai et al. [26] also demonstrated this transient phenomenon by a large-scale study of the cutting forces in a face milling, i.e., intermittent cutting with a single cutting edge. It was found, however, that this transient character extended over a longer stretch of the $F(t)$ force–time curves. It was also observed that the time curve of the detected cutting force $F(t)$ does not end in a break at the end of the milling cycle. Although there is no actual cutting, the detected signal has a gradual decay rather than a discontinuity. Its duration was found to be comparable to the length of the initial transient phase.

The analysis of the results led to the realization that the measurement technique of short-time cutting functions as a dynamic mechanical-electronic system that influences the detected signals. And its operation is not limited to the time of chip removal, because a non-zero signal is detected even after material removal. This decay of the measurement system is obviously energetically related to the active measurement process. The task in the second phase of the research presented here was to investigate the regularity with which the actual cutting force, as an input signal, will be mapped at the output of the measuring system. A further important question was how to deduce the input signal of the actual cutting force from the transient signal detected at the output of the measuring system. To study this, the aim was to develop a mathematical model that can be used to link the initial transient phase of the cutting process with the decay.

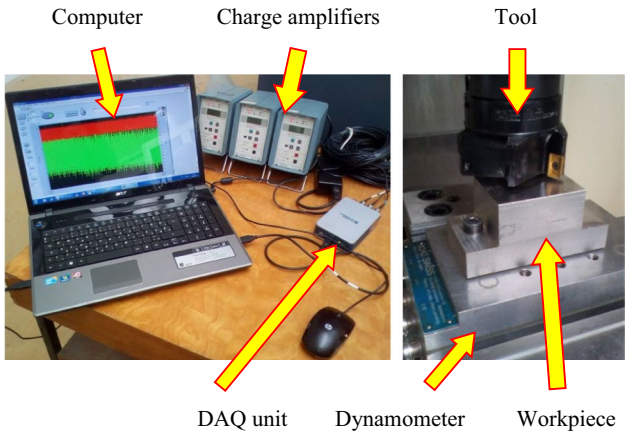

Fig. 1 The force measuring system

2 The technical characteristics of the measuring system and the experimental program

The cutting experiments were carried out for symmetrical face milling with both up- and down-milling methods. During the force measurement, a single insert was attached to the milling head.

2.1 Technical characteristics of the measuring system

The elements of the force measuring system are shown in Fig. 1, which are as follows:

- Kistler 9257A type three-component dynamometer;
- Kistler 5011A type charge amplifiers (3 pcs);
- National Instruments CompactDAQ-9171 type four channel data acquisition unit;
- Notebook with the measurement software created in the LabView programming language.

The workpiece was fixed to the flat surface of the dynamometer through two holes with screws. As a result of the force applied to the workpiece, the dynamometer generates electrical signals corresponding to the *xyz* directions interpreted in the Cartesian coordinate system. After that, the magnitude of the signal is converted per channel by a charge amplifier according to the set gain value. Then the three amplified independent signals are sent to the data collection unit, where the analog/digital signal conversion takes place for further computer processing. There are shielded cables with BNC connectors from the dynamometer to the data collection unit, and a serial connection cable leads from the data collection unit to the USB port of the computer.

Since during milling—due to the rotating movement of the tool—the thickness of the chip is not constant, but changes continuously, so it is of great importance how the tool and the workpiece are positioned relative to each other during cutting, and how they move relative to each other. Figure 2 illustrates the arrangement of the tool and the workpiece in the case of the three types of milling methods (symmetrical, down-, up-milling), the characteristic values of the kinematics, and φ angles are also indicated. The *xyz* coordinate directions are also specified. Chip removal takes place between points *A* and *B* of the workpiece. *A* is the point of entry into cutting, *B* is the point of exit from cutting. So, according to Fig. 2, in up-milling, cutting starts at $\varphi = 0°$ and ends at $\varphi = 90°$, while in down-milling, it starts at $\varphi = 90°$ and ends at $\varphi = 180°$. In symmetrical milling, the location of entry and exit into the cutting is determined by the width of the milled surface and the diameter of the tool. As an example, Fig. 3 shows the values of the main cutting force F_c for the three types of milling as a function of the angle φ; the diagram is based on the cutting forces measured during machining with one of the experimental settings (C45, $a_p \cdot f_z = 0.4 \cdot 0.1$ mm^2, $v_c = 200$ m/min).

2.2 Conditions for the cutting experiments

The measurements were made in the laboratory of the Institute of Manufacturing Science of the University of Miskolc,

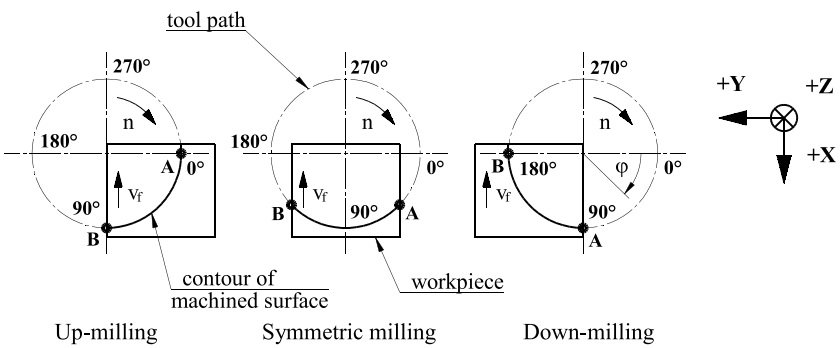

Fig. 2 Interpretation of φ(t) and the x, y, z coordinate system used in the measurements

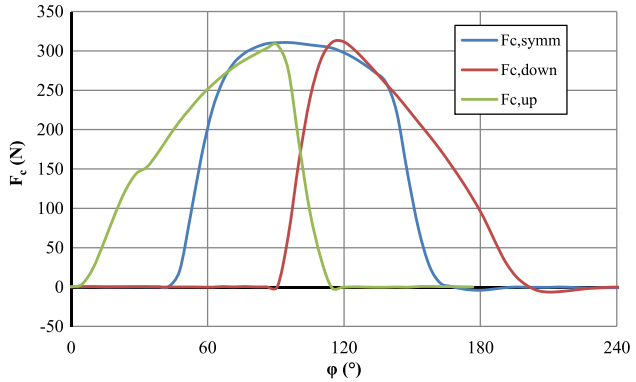

Fig. 3 The measured $F_c(\varphi)$ curves

with a PERFECT JET MCV-M8 (H) type vertical machining center.

The type of the milling head: Sandvik R252.44–080027-15 M face milling cutter, $D = 80$ mm.

The type of the milling insert: Sandvik R215.44-15T308M-WL GC4030.

Cutting edge characteristics: $\alpha = 11°$, $\gamma = 20°$, $\lambda_s = 4°$, $\kappa_r = 90°$, $\kappa_r' = 3°$, $r_\varepsilon = 0.8$ mm.

The measurements carried out during the research covered a wide spectrum of technological parameters:

machining method	symmetrical, down- and up-milling.
steel material quality	C45 (1.0503) and X5CrNi18-10 (1.4301).
cutting speed	$v_c = 50 \ldots 450$ m/min.
feed	$f_z = 0.1 \ldots 1.6$ mm/rotation.
depth of cut	$a_p = 0.4$ mm.
specimen width	$B = 21.4$, 40, and 58 mm.

2.3 Steps of the investigations

The investigation of the transient change of the cutting force and the development of the theoretical model of the actual cutting force were carried out in the following steps. In the experiments performed under the specified (chosen) conditions, the transient change in the cutting force between the initial transient nature of the milling cycle and the decay was analyzed by choosing a mathematically analyzable analog circuit for the electro-mechanical system of force measurement. Based on the close relationship revealed between the initial transient nature of the milling cycle and the decay, the cutting and measurement were further investigated as a complex electro-mechanical system. As a result, a mathematical model was developed, and the model was validated with experimental data.

3 Experimental analysis of the decay process following the cutting phase

For all measurements presented in this study, the cutter was equipped with only one cutting edge. It would make the evaluation of the measurement results uncertain if two (or more) inserts were to be cutting at the same time when using a milling cutter with several inserts. The evaluation of the obtained results also extended to the period following the cutting stage, when the measurement system detected a decay process. Figure 4 shows the detected curves of the cutting force components F_x, F_y, and F_z for down-milling of C45 steel (C45, $a_p \cdot f_z = 0.4 \cdot 0.4$ mm^2, $v_c = 150$ m/min, B/D = 58/80 mm/mm). The detected decay after the end of the cutting cycle (indicated by dashed lines) can also be seen in the figure, which shows undulations.

Even though chip removal only occurs in the angular position of the cutter $90° < \varphi < 180°$, it is obvious from energetic considerations that the data detected in the $180° < \varphi$ angle range of the force register must also be taken into account when evaluating the data. It can be seen that the measuring system indicated forces greater than zero here as well. Therefore, the investigations reported in this study also covered the information detected in the decay phase.

This can be seen more clearly in Fig. 5a, which contains the results of measurements made during symmetrical milling (X5CrNi18-10, $a_p \cdot f_z = 0.4 \cdot 0.4$ mm^2, B/D = 58/80 mm/mm, $v_c = 150$ m/min). By enlarging the decay section in Fig. 5b, it can also be seen that the amplitude of the ripple decreases rapidly due to the strong damping built into the measuring system. It is also worth considering here that the cutting force was measured by measuring the force components in the x, y, and z directions attached to the workpiece which was fixed to the table of the machine. Consequently,

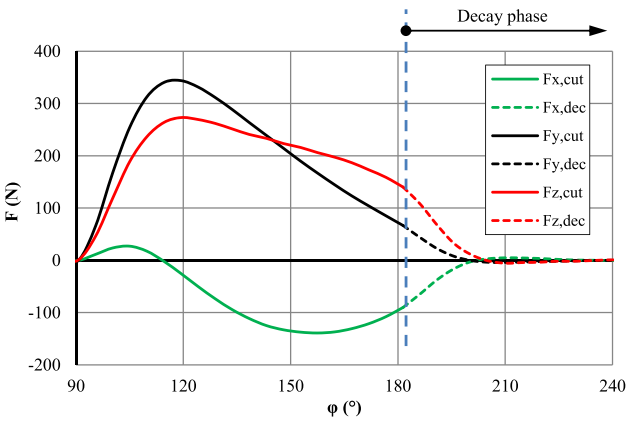

Fig. 4 The detected values of the cutting force in the x, y, and z directions in down-milling, as a function of the rotation angle of the cutter φ

the force components F_c and F_f are the values calculated from the measured data F_x and F_y.

Figure 6 shows the force values measured during symmetric milling with different feed rates C45, $a_p = 0.4$ mm, B/D = 58/80 mm/mm, $v_c = 150$ m/min) and the sections detected at the time of decay. It is clear that on the $F_y(t)$ force curves detected at different feed rates, the end of cutting and the beginning of the decay occurred at the same t_{cut} time. Of course, in the case of different feeds, the detected force is very different. Despite this, it can be established that the curves intersect the time-axis t at almost the same place during the fast decay phase. This can also be seen enlarged in Fig. 6b.

One more observation can be made about this series of measurements. Figure 7a shows the specific values of the decay when the decay data detected at different feeds are divided by the value detected at the end of cutting: $F_{y,dec}(t)/F_{y,cut}$, (C45, $a_p = 0.4$ mm, B/D = 58/80 mm/mm, $v_c = 150$ m/min). As shown in Fig. 7b, the curves are practically overlapping. It is obvious that the decay is independent of the value of the feed. It is also a remarkable fact that the decay dynamics are practically the same. This can probably only be traced back to the dynamic characteristics of the electro-mechanical measuring system. This finding is confirmed by Fig. 6b, which illustrates the undulation observed in the second phase of the decay. This also shows that the zero points of the undulation and the wavelength are practically the same even in the case of very different feed values.

This confirms the finding that the forces detected during decay are already independent of the forces detected during cutting from the final time of the cutting phase t_{cut}. In other words, they only depend on the specifics of the measurement system.

A similar conclusion can be made for the $F_z(t)$ curves detected at different cutting speeds. For the measurements

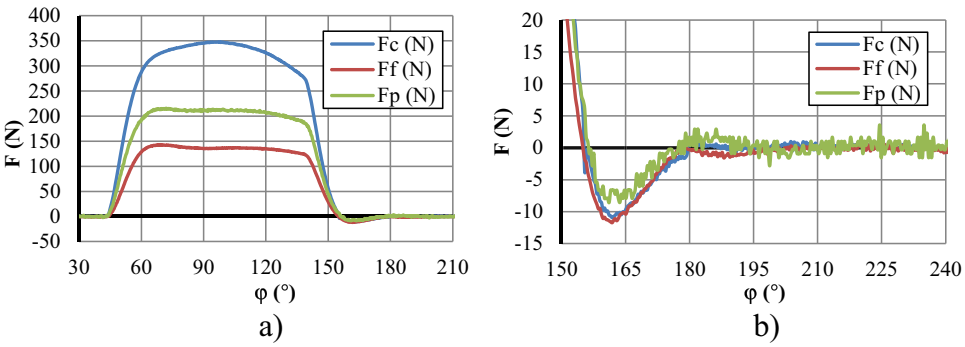

Fig. 5 Cutting forces measured during symmetrical milling of X5CrNi18-10 steel

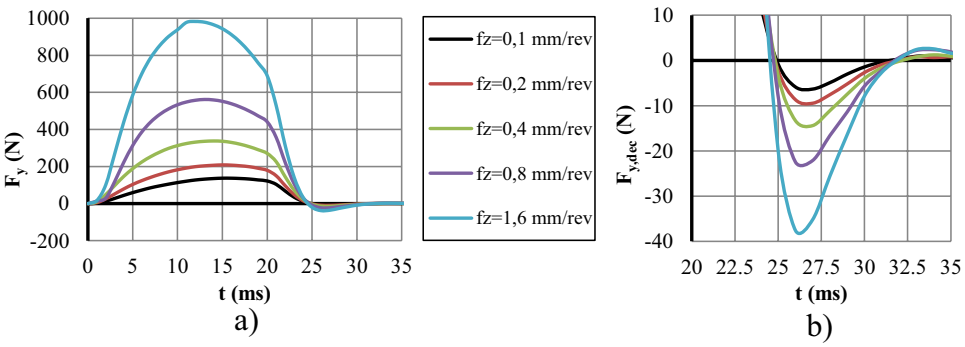

Fig. 6 In the case of symmetrical milling, a Fy(t,f_z) component of the cutting force measured in the y direction and b $F_{y,dec}$ section detected during decay after cutting

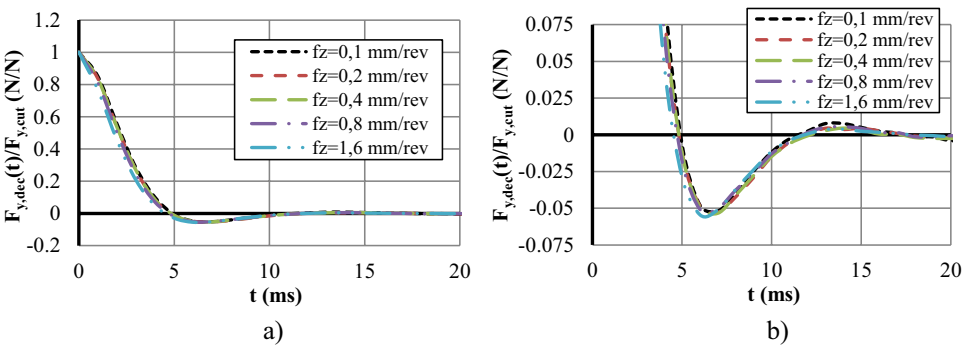

Fig. 7 The specific value of the $F_{y,dec}(t,f_z)$ curves shown in Fig. 6 compared to the $F_{y,cut}$ value detected at the beginning of the decay

made on C45 steel, Fig. 8a, which summarizes the complete cutting cycles, and Fig. 8b, which highlights the decay sections, show very similar characteristics for the different cutting speeds (C45, $a_p \cdot f_z = 0.4 \cdot 0.4$ mm^2, B/D = 21.4/80 mm/mm).

The coordinates of the essential points of the $F_z(t)$ curve are shown in Table 1, the interpretation of which can be seen in Fig. 9a and b (C45, $a_p \cdot f_z = 0.4 \cdot 0.1$ mm^2, B/D = 21.4/80 mm/mm). The points 0, 3, 5, 7, 9, 11, and 13 are the zero points of the function, while the points 1, 4, 6, 8, 10, and 12 are the locations of the local extreme values of the function. Figure 9a illustrates the sections of the curve. S_{cut} denotes the cutting phase (between points 0 and 2), the initial phase of the decay is denoted by $S_{dec,i}$ (between points 2 and 3, between the exit from the workpiece and the first zero position), the wavy phase of the decay is denoted by $S_{dec,w}$ (between points 3 and 13). The details of the ripple at the decay of the detected force F_z are illustrated separately in Fig. 9b. The first wave period ($S_{dec,w1}$: section between points 3 and 7) and the second wave period ($S_{dec,w2}$: section between points 7 and 11) were marked in the wavy phase of the decay.

An important characteristic of this series of measurements is that the width of the specimen machined by the D = 80 mm diameter milling cutter was B = 21.4 mm. This had the advantage that the thickness of the removed layer changed during the rotation of the cutter, but this change compared to the average was less than 1.5%. Thus, in this case, the removed cross section can be considered constant with a good approximation even during milling.

The effect of cutting speed was also investigated when milling X5CrNi18-10 quality steel. Figure 10a shows the data obtained during the measurement of the F_z component during symmetrical milling ($a_p \cdot f_z = 0.4 \cdot 0.4$ mm^2, $B/D = 21.4/80$ mm/mm). The decay phase can also be seen separately in Fig. 10b. Based on these, it can be concluded that the nature of the curve of the detected data during decay is the same for the two tested steels.

Similar measurements were also made for down-milling. As shown in Fig. 11a and b, the curve sections detected

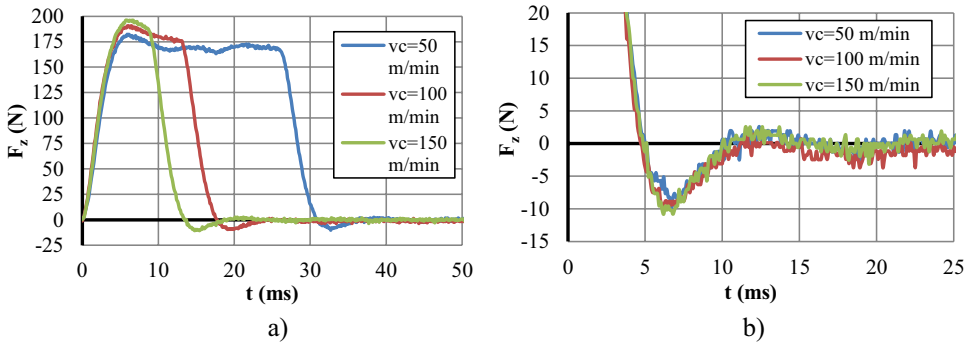

Fig. 8 Results of force measurements a during milling at different cutting speeds and b wavy phase of the decay

Table 1 Characteristic values of the forces $F_{z,i}(t_i)$ detected at a speed of $v = 150$ m/min (see Fig. 9)

No	0	1	2	3	4	5	6	7	8	9	10	11	12	13
t_i (ms)	0	6.2	8.6	13	15.1	19.2	21	24.8	26.9	30	33.2	36.5	38.4	40.4
$F_{z,i}$ (N)	0	196	188	0	− 10	0	1.6	0	− 0.9	0	0.7	0	− 0.9	0

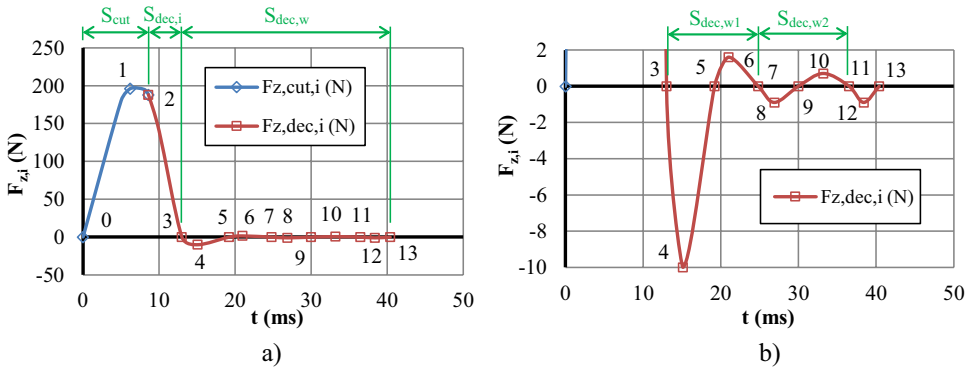

Fig. 9 Characteristic points of the $F_z(t)$ force curve measured for $v_c = 150$ m/min a in the cutting and decay phases and b in the wavy section of the decay phase

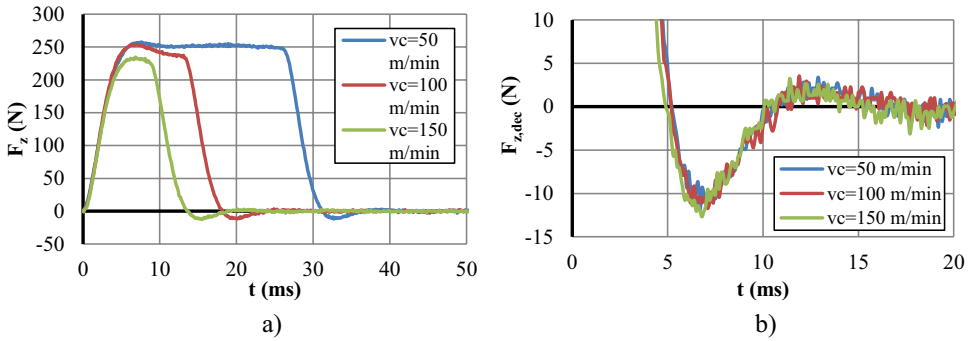

Fig. 10 The effect of the cutting speed on the cutting force F_z a during symmetrical milling of X5CrNi18-10 steel and b the undulating detail of the decay

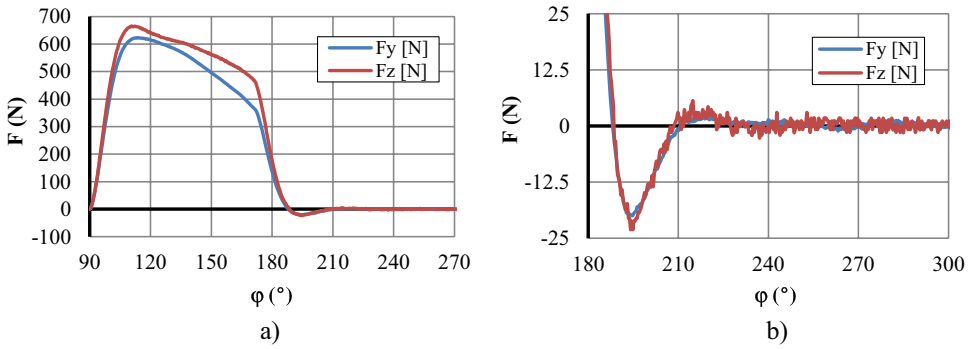

Fig. 11 Comparison of the F_y and F_z components of the cutting force in down-milling of X5CrNi18-10 quality steel

during the decay phase completely coincide with the components of the cutting force F_y and F_z (a_p·f_z = 0.4·0.4 mm^2, B/D = 58/80 mm/mm, v_c = 150 m/min).

On the basis of Figs. 4, 5, 6, 7, 8, 9, 10, and 11 illustrating the measurement results, it can be concluded that, regardless of the technological data (feed and cutting speed) and the quality of the tested steel, the main parameters of the detected decay and the subsequent undulation on the time scale t are close to the zero locations and the locations of the force extremes, so the wavelengths are almost the same. These should therefore be classified as important parameters of the measurement system, which are independent of specific measurements.

When examining the measurement results, it is also striking that the characteristics of the initial stage of the chip removal cycle are very similar to the curves that can be detected during its decay. Figure 12a illustrates this fact for C45 steel at a cutting speed of v_c = 150 m/min (a_p·f_z = 0.2·0.4 mm^2, B/D = 21.4/80 mm/mm). The figure shows the steps of a mapping that results in the decay curve being superimposed on the initial, ascending stage of chip removal. The thick decay curve with index "dec" is mirrored on the axis parallel to the t-axis at a distance $F_{cut,max}/2$ ("dec-mirr": decay-mirror), and then the resulting curve is shifted back on the t-axis until the beginning of the chip removal ("dec-mirr-move": decay-mirror-move). The similarity of the two curves in the overlay is striking. This fact is confirmed by Fig. 12b, which shows the correlation of the two overlapped curves. As can be seen, practically R^2 = 1. An important feature of this series of measurements is that they were taken when milling a specimen of width B = 21.4 mm, when the thickness of the removed layer can therefore be considered constant.

Figure 13 was made based on force measurement at a cutting speed of v_c = 300 m/min (C45, a_p·f_z = 0.2·0.4 mm^2, 21.4/80 mm/mm). In this case, due to the higher cutting speed, the tool cut through the workpiece so quickly that the transient wave rising at the beginning of the operation could not even reach its first maximum. The decay started earlier. Nevertheless, the phenomenon seen in Fig. 12 can also be observed here. The decay curve can be mirrored and moved onto the rising section of the cut. The correlation between the curve sections detected at the beginning of the cutting and at the decay is also close here (Fig. 13b).

The studies in which the development of the difference ratio of the cutting force $\Delta F_c/\Delta t$ was studied as a function of the cutting time led to a similar conclusion. Figure 14a shows the result of such an analysis for X5CrNi18-10 steel at a cutting speed of v_c = 150 m/min (a_p·f_z = 0.4·0.4 mm^2, B/D = 21.4/80 mm/mm, sampling frequency 100 kHz). In this case, the values detected during the decay ($\Delta F_{c,dec}/\Delta t$) were mirrored directly on the t-axis and then shifted back until the start of the cutting cycle ($\Delta F_{c,dec\text{-}mirr\text{-}move}/\Delta t$). It can also be seen that the data of cutting and decay mapped in this way also show a close correlation according to Fig. 14b (R^2 = 0.9575).

The close relationship between the force detected at the initial stage of cutting and the decay is also illustrated in

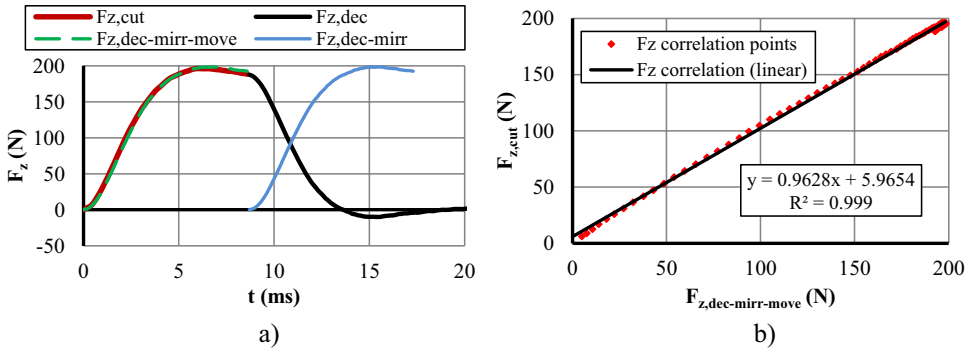

Fig. 12 Mirroring the decay curve detected during the force measurement onto the curve of the cutting section. a The steps of mirroring. b Correlation between data detected during cutting and decay

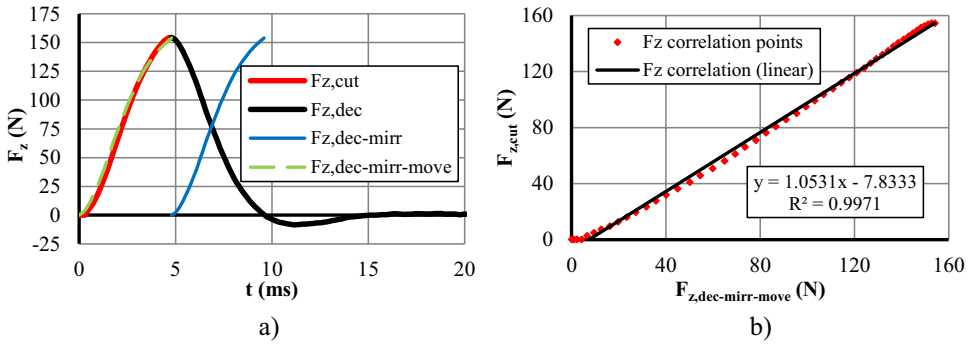

Fig. 13 Mirroring the decay curve detected during the force measurement onto the curve of the cutting process. a The steps of mirroring. b Correlation between data detected during cutting and decay

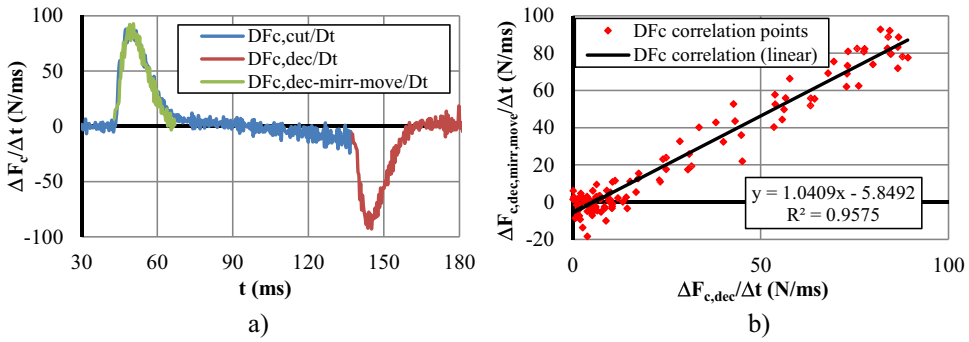

Fig. 14 Differential quotient of the cutting force detected during symmetric milling in the cutting phase ($\Delta F_{c,cut}/\Delta t$) and during decay ($\Delta F_{c,dec}/\Delta t$). a The initial phase and the mirrored and moved decay phase overlapped. b Correlation

Fig. 15, which also shows the initial stage of the cutting process shown in Fig. 14a enlarged. This clearly shows the close connection between the initial transient phase and the decay.

In the case of the two investigated materials, C45 unalloyed C-steel and highly alloyed X5CrNi18-10 steel, the process of chip removal is significantly different. This is illustrated in Fig. 16, which shows the longitudinal section of the chips produced with the two materials ($a_p \cdot f_z = 0.2 \cdot 0.4$ mm^2, $v_c = 200$ m/min). It can be seen that the well-known lamellar chip produced in X5CrNi18-10 steel is significantly different from the chip in C45 steel. Less and very strongly deformed layers follow each other, and the deformation and stress conditions during their formation are obviously very different. It has emerged that the cutting force can also fluctuate strongly during the formation of such a chip. To verify this, Figs. 14 and 15 show the results of measurements where the sampling frequency was 100 kHz. This served the purpose of detecting possible fluctuations in the cutting force. Based on the two figures, however, not only that can be established that the decaying phase of the measurement can be overlapped with the initial phase of the force curve, but also that the periodic high deformation fluctuation visible on the chip section is not followed by the detected force data at all.

These investigation results clearly show that the transient characteristic detected during force measurements in the initial stage of cutting is primarily determined by the dynamic parameters of the measuring system. It was established that the values of the decay dynamics, i.e., the important times, are practically independent of the value of the F_{cut} force detected at the end of the active cutting process. These are the time-data $t_{n,i}$ typical of the

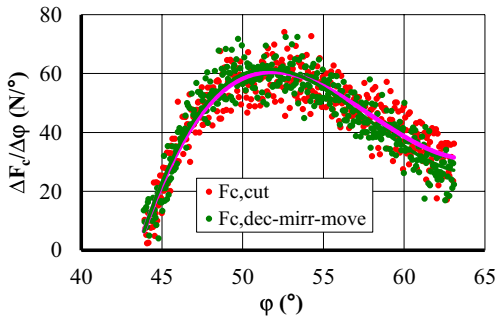

Fig. 15 Detail of Fig. 14a, where the cutting and decay sections are overlapped

measuring system, for which the detected force is zero, i.e., the registered, undulating force curve $F_{dec}(t)$ intersects the t-axis; such points are t_{n1}, t_{n2}, t_{n3}. Further zero points of the curve (e.g., t_{n4}) are already uncertain due to the rapid decay. The essential characteristic of the measuring system is the first force minimum (t_{min1}) time on the decay curve. The corresponding $F_{dec,min1}$ value already depends on the F_{cut} value. Another important characteristic, the angular velocity Ω of the decay ripple, can be determined from these time data.

The decay that always follows the active phase of the force measurement therefore contains important information that can be used to determine the actual cutting force. Table 2 contains a statistical summary of the parameters measured during the entire decay measurement series.

Another important finding from the results of the measurements is that the transient phenomenon experienced at the beginning of the cutting phase is related to the dynamics of the decay. This relationship is close. This is shown by the measurements in which the removed layer thickness was considered constant (in case of $B/D = 21.4/80$ mm/mm at $< 1.5\%$). Therefore, the force curve measured during the initial, transient phase of cutting was a direct reflection of the curve detected during decay.

Table 2 Statistical aggregation of the results of force measurements

	t_{n1} (ms)	t_{min1} (ms)	t_{cikl} (ms)
Mean	5.04	6.6	12.1
Minimum	4.57	6.5	10.1
Maximum	5.4	7	14.1
Average deviance	0.2	0.33	0.91
Variance	0.24	0.42	1.16

4 Model of the electro-mechanical system of force measurement

The analysis of the previously presented measurement results led to the realization that the short-time cutting measurement technique functions as a dynamic mechanical-electronic system that not only amplifies but also influences the signals detected on the force measurement cell. The effect is not limited to the time of chip removal, because there is also a non-zero detected signal at the output of the measuring system. This decay of the measurement system after material removal is energetically obviously connected to the active measurement process.

The following is based on the strong simplification that the entire measuring system can be reduced to a series RCL circuit with R ohmic, C capacitive, and L inductive resistances. The behavior of such circuits can be described by the well-known equation below (Eq. 1).

$$u(t) = L\frac{d}{dt}i(t) + \frac{1}{C}\int_0^t i(t)dt + Ri(t) \tag{1}$$

The following analysis is based on the additional assumption that the chip removal is intermittent but with constant technological parameters. This condition can be easily approached with a small B/D ratio for symmetrical milling. Thus, Eq. 1 can be transformed into the following linear equation, where C_{part} is a constant.

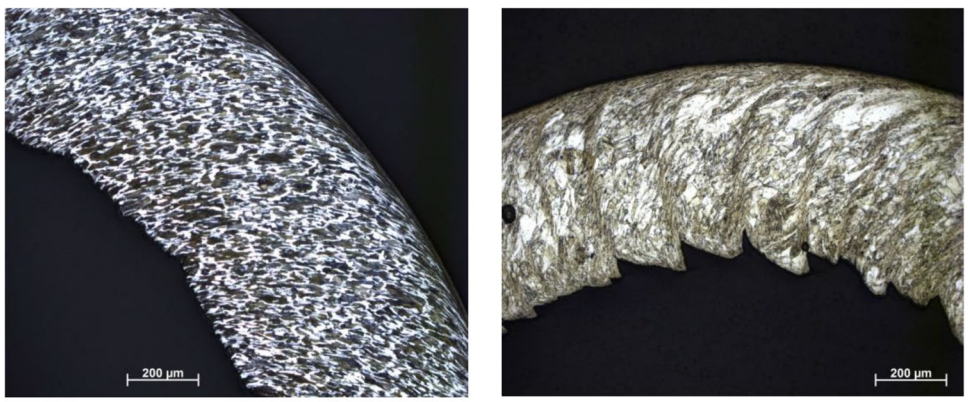

a) b)

Fig. 16 Microscopic images of the structure of the chips produced during milling. a C45. b X5CrNi18-10

$$\frac{d^2F}{dt^2} + \frac{R}{L}\frac{dF}{dt} + \frac{R}{\sqrt{LC}}F = C_{part} \tag{2}$$

Two cases should be examined here:

a) $C_{part} = 0$, in which case Eq. 2 is homogeneous, and describe the decay process.
b) $C_{part} > 0$, which refers to its chip removal.

It should be noted that Eq. 2 also contains some further simplification, because the capacitance C, and especially the self-inductance L, can change during the saturation of the circuit. This is ignored here for now.

Introducing the notations of

$$\frac{R}{L} = \frac{2}{\tau} \tag{3a}$$

and

$$\frac{R}{LC} = {\omega_0}^2 \tag{3b}$$

the form of Eq. 2 for case a) is as follows:

$$\frac{d^2F}{dt^2} + \frac{2}{\tau}\frac{dF}{dt} + \omega_0^2 F = 0 \tag{4}$$

where τ is the time constant characteristic of damping, and ω_o is the self-frequency of the resonant circuit modelling the decay.

The well-known solution of Eq. 4 is a time-decreasing amplitude wave, which can be described by the function:

$$F(t) = C_F \exp\left(-\frac{t}{\tau}\right)\sin\left[\Omega\left(t - t_1\right) \pm (2k+1)\pi\right] \; k = 0, 1, 2 \tag{5}$$

Here, Ω is the natural circular frequency of the undulation that develops during decay, which can be calculated as follows:

$$\Omega = \sqrt{{\omega_0}^2 - 1/4\tau^2} \geq \frac{1}{4\tau^2} \tag{6}$$

Here ω_0 is the natural frequency of the entire complex electromechanical system. This wave Ω, which can be determined based on the measurements, can be calculated by knowing the self-frequency and the time constant τ.

The data required for further calculations can be read from the decaying section of the detected $F(\omega t) = F(\varphi)$ curve:

- the force F_{cut} at the end of the cutting phase or at the beginning of the decay at the time t_{cut},
- the zero points of the decaying wave curve t_{n1}, t_{n2}, t_{n3}…, which are detected by the measuring system at the values $F = 0$,
- the time t_{min1} of the first F_{min1} force minimum of the force curve detected at decay,

The constants of Eq. 5 can be determined from these data.

The decay is characterized by the circular frequency Ω, and the corresponding phase angle Φ is independent of the rotation of the cutter, since there is no cutting during the decay. This is the internal self-motion of the measuring system. When examining the decay process, it is therefore necessary to take into account the fact that two coordinate systems can be interpreted there. Based on the cutting speed v_c, the rotation speed n of the milling head and the angular rotation φ determine a circular frequency ω. And the angle step $\Delta\varphi$, arbitrarily chosen during the investigations, results in a time step $\Delta t = 2\pi/\Delta\varphi$, which is the time scale of both movements—cutting and decay. The circular frequency ω resulting from the rotation speed of the milling head works like a "metronome."

The phase angle Φ is determined by the circular frequency Ω from time t_1. At the moment when $F = 0$ during the decay, that is, $t = t_n$, the angular position of the decay is $\Phi_1 = \Omega \cdot t_1$ due to Eq. 5. Denote this state in the cutter's coordinate system by $\varphi_{n,1}$, then here $t_1 = \varphi_{n,1}/\omega$. All in all:

$$\frac{\Phi_1}{\Omega} = \frac{\phi_{n,1}}{\omega}$$

And since for $t = {}_{tn,1}$ from Eq. 5:

$$\sin\left[\Omega\left(t_{n,1} - t_1\right) \pm (2k+1)\pi\right] = 0 \; k = 0, 1, 2 \tag{8}$$

therefore:

$$t_1 = t_{n,1} \pm \frac{(2k\pi + 1)}{\Omega} \tag{9}$$

Taking all of this into account, the solution of Eq. (2) can be brought to the following form, which is the solution of the homogeneous version of Eq. (5) $C_{part} = 0$.

$$F_{dec}(t) = C_F \exp\left(-\frac{t - t_{cut}}{\tau}\right)\sin\left[\Omega(t - t_{n,1}) + (2k+1)\pi\right] \; k = 0, 1, 2 \ldots \tag{10}$$

This gives the curve detectable at the decay starting at time $t = t$cut.

Version (b) corresponds to the start of the cutting process, where the electrical signal of the force measurement cell is $C_{part} > 0$. From Figs. 10, 11, 12, 13, and 14, it was observed that the force-registration curve of the cutting is a peculiar two-step mapping of the curve obtained at the decay:

- mirroring the function F_{dec} (10) on the line parallel to the t-axis, $F_{ax} = F_{cut}/2$,
- pushing back the mirrored curve with time t_{cut} on the t-axis.

According to this, the force detected in the cutting stage is:

$$F(t) = F_{dec}(t = t_{cut}) - F_{dec}(t) \tag{12}$$

At the beginning of the decay phase, the exponential term drops out, therefore according to Eq. (10).

$$F_{dec}(t = t_{cut}) = F_{cut} = C_F \sin\left[\Omega(t_{cut} - t_{n,1}) + (2k+1)\pi\right] \; k = 0, 1, 2 \ldots \tag{13}$$

Introducing the

$$C_\Omega = \frac{1}{\sin\left[\Omega(t_{cut} - t_{n,1}) + (2k+1)\pi\right]} \tag{14}$$

notation, $C_F = F_{\text{cut}} \cdot C\Omega$

Thus, from (12), the force formula valid for the cutting section, which can be proven to also be a solution to Eq. (2):

$$F(t) = F_{cut}\langle 1 - C_\Omega \exp(-\frac{t}{\tau}) \sin\left[\Omega(t - t_n) + (2k+1)\pi\right]\rangle \; k = 0, 1, 2 \tag{15}$$

As already mentioned, the starting assumption of this mathematical model was that the technological parameters were unchanged throughout the cutting cycle. The constants F_{cut}, C_Ω, τ, Ω, and t_{n1} in formula (10) can be determined from the registers obtained during the force measurement.

The cycle time of the decay can be calculated from one of the relationships $t_{\text{cikl}} = t_{\text{min2}} - t_{\text{min1}} = t_{\text{n3}} - t_{\text{n1}}$, so the circular frequency of the decay is as follows:

$$\Omega = \frac{2\pi}{t_{cikl}} \tag{16}$$

When determining the time constant τ, it is advisable to start from the fact that the first minimum $F_{\text{min1}}(t = t_{\text{min}})$ of the undulating force registered at the decay can be measured well (see Figs. 6, 7, 8, and 10). Omitting the details, this results in the following:

$$\tau \cong \frac{1}{\Omega}\langle tg\left[\Omega\left(t_{\text{min}} - t_{n1}\right) \pm 2k\pi\right]\rangle \; k = 0, 1, 2 \ldots \tag{17}$$

It should be noted that the time constant τ calculated with formula (17) characterizes the initial, fast phase of the decay. It should be taken into account that the coefficients in Eqs. (1) and (2) were assumed to be constant in the mathematical model. This is justified in the case of negligibly small inductance, but then a linear differential equation with a first-order constant coefficient would result, the solution of which has no wave motion. However, this can be observed in the present case. The first, very fast phase of the decay is followed by a more slowly diminishing, low-intensity wave. The latter subsides quickly, but at the beginning of the detected decaying force curve, a wave of technically perceptible magnitude still appears. This should also be taken into account when evaluating force measurements over a short period of time. Here, the time constant $\tau = \tau_\Omega$ can be calculated from the quotient of the first two power minima detected during decay $F_{\text{min2}}(t_{\text{min2}})/F_{\text{min1}}(t_{\text{min1}})$:

$$\tau_\Omega = -\frac{t_{cikl}}{\ln\ F_{\text{min}\,2}/F_{\text{min}\,1}} \tag{18}$$

In summary, using (2) and (4)—from the data detected in the decaying idling phase—the following can be determined regarding the dynamic electronic characteristics (R, C, and L) of the entire measuring system:

$$\frac{L}{R} = 2\tau \tag{19a}$$

$$\frac{L}{\text{RC}} = \Omega^2 - \left(\frac{1}{2\tau}\right)^2 \tag{19b}$$

Therefore, two equations can be formed for the three parameters. If the self-induction in the measuring system depends on the magnetic saturation of one of the components, then this mathematical model can only be used to a limited extent.

The model can also be used to analyze the energetic characteristics of the process. The momentum of the actual cutting force F_{fact} causing chip removal during time $t = \varphi/\omega$

$$\text{I}(t_{cut}) = \int F_{fact}(t)dt \cong \sum_{t0}^{tcut} F_{fact}(t)\Delta t = \frac{1}{\omega}\sum_{\phi 0}^{\phi cut} F_{fact}(t)\Delta\phi \tag{20}$$

According to the law of conservation of momentum, this must be identical to all the momentum that are detected during the measurement during the entire cycle, i.e., during cutting and decay.

$$\text{I}_{fact}(t_{cut}) = \sum_{\phi 0}^{\phi cut} F(\phi)\Delta\phi \cong \text{I}_{meas} = \sum_{\phi 0}^{\phi cut+\phi dec} F(\phi)\Delta\phi \tag{21}$$

Since the work and momentum during the operation are closely related according to the simple relationship $L = I \cdot v_c$, the specific energy requirement Q for the chip with volume V can be calculated as follows:

$$Q = \sum I \cdot v_c / V \tag{22}$$

Based on this, the different milling methods can be compared even if determining the actual value of the maximum cutting force is problematic.

5 Validation of the mathematical model

The decay of the detected cutting force F starts with the value F_{cut} at the time t_{cut} of the end of chip removal. The solution (10) of Eq. (4) written for this process contains three constants: the first zero point t_{n1} of the decay curve and the two calculated values determined by the force measurements, the self-frequency Ω of the undulating part of the decay, and the time constant τ of the first, fast phase of the decay. In order to determine these, the following characteristic times on the time-axis t of the $F_{dec}(t)$ force curve detected at decay are read: t_{n1} and t_{n3} are the first and third intersection points of the decay curve, t_{min1} and t_{min2} are the first and second minima of the $F_{dec}(t)$ curve, respectively. Using them, the cycle time t_{cikl} of the wave can be calculated from these data, while Ω can be calculated from Eq. (16). Knowing these, the function C_Ω constant of (10) can then be determined using Eq. (14), and τ can be determined using $C_F = F_{cut} - C_\Omega$ using formula (17).

In one set of measurements, a symmetrical milling of a $B = 21.4$ mm wide band was carried out using a milling cutter with a diameter of $D = 80$ mm. With these dimensions, it was possible to minimize the problem typical of milling that the thickness of the removed layer changes. In this particular case, the maximum deviation of the thickness of the removed layer compared to the average was less than 1.5% and thus could be ignored. Figure 17 was constructed using the measurement results presented in Fig. 8 by fitting the average of the three versions of the cutting speed v_c to the curve calculated by Eq. (10). As shown in Fig. 17b, the calculated values of the F_z force closely match the measured values. Figure 18 was also created using this series of measurements, which shows how the $F_{z,dec}(t)$ curve calculated for decay using formula (10) fits the $F_{z,cut}(t)$ function measured during cutting at the beginning of the cutting cycle (C45, $a_p \cdot f_z = 0.4 \cdot 0.1$ mm^2, B/D = 21.4/80 mm/mm, $v_c = 150$ m/min).

According to the measurement results presented in Chapter 3, the transient force detected during active cutting during milling is closely related to the measurement results detected during decay. It follows that the curve calculated with function (15), which fits the decay data, is also closely correlated with the initial transient measurement results (Fig. 18b). Using formulas (10) and (15), the entire measurement cycle can then be calculated, as shown in Fig. 19 (C45, $a_p \cdot f_z = 0.4 \cdot 0.1$ mm^2, B/D = 21.4/80 mm/mm, $v_c = 150$ m/min). Figure 19b shows that the small hysteresis in the operation of the measuring system can be detected, which was referred to in formulas (19). However, this is so small that it can be ignored when evaluating the measurements.

Similar results were obtained for the symmetrical milling of KO33 steel. Figure 20 shows the close fit of the measured and calculated values of the force F_z during decay, and Fig. 21 shows the similarly close relationship between the averaged results measured during cutting (see Fig. 12) and the curves calculated for decay at three values of the cutting speed v_c.

With these measurement results, it can be considered proven that the actual cutting force can be calculated with functions (10) and (15) in the case of intermittent cutting, in the case of removal of a layer of uniform thickness. According to Fig. 19b, the fit of the measured and calculated curves is close. This finding is confirmed by Fig. 22, which illustrates the fit of the difference ratios $\Delta F_z/\Delta t$. This is remarkable because the standard deviation of the ΔF differences due to the measurement results is usually quite large. Nevertheless, the fit between the calculated and measured data is close.

Functions (10) and (15) are complex, with an initial transient phase followed by a wave whose amplitude then decreases further. Table 3 contains the relevant measurement data. Here, the decay ripple takes into account the overlapping intervals t_{min} and t_{max}. The prolongation of the decay process in the wave phase is clearly visible. This is the reason why it is sufficient to consider at most two waves in the detected results of the force measurement (Fig. 23).

In conclusion, the electro-mechanical characteristics of the measurement system can be summarized in Table 4 based on the results of the measurement series.

Based on all of this, it can be concluded that formula (10) describes the decay process in accordance with

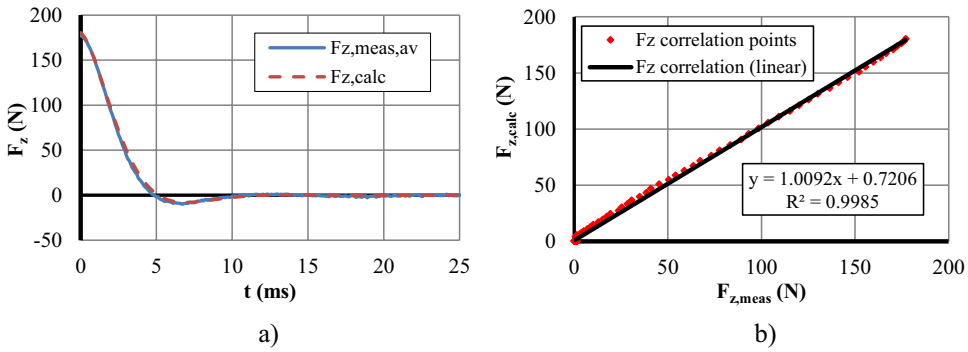

Fig. 17 Calculated curve fitted to the average of the measurement results shown in Fig. 8. **a** Calculated curve fitted to the average of F_z forces measured at three cutting speeds. **b** Correlation of measured and calculated data

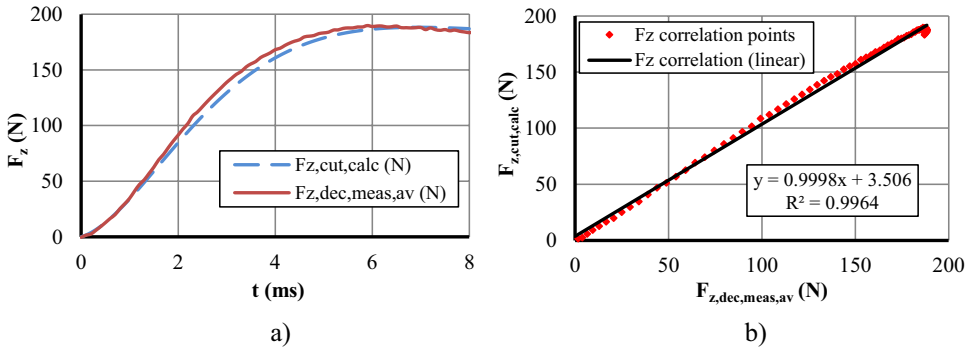

Fig. 18 Relationship between data detected at the beginning of symmetrical milling and the curve calculated based on function (10). **a** Measurement and calculation results. **b** Correlation

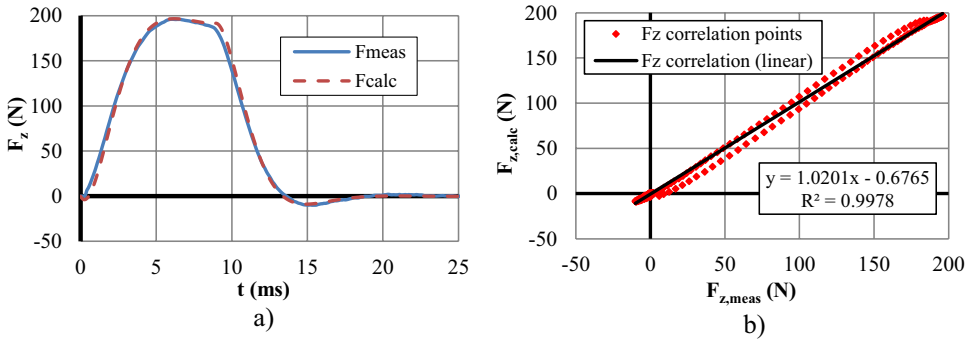

Fig. 19 Fitting the calculated $F_z(t)$ curve to the measured values for a complete cutting cycle (see Fig. 20). **a** The measured and calculated curves. **b** Correlation

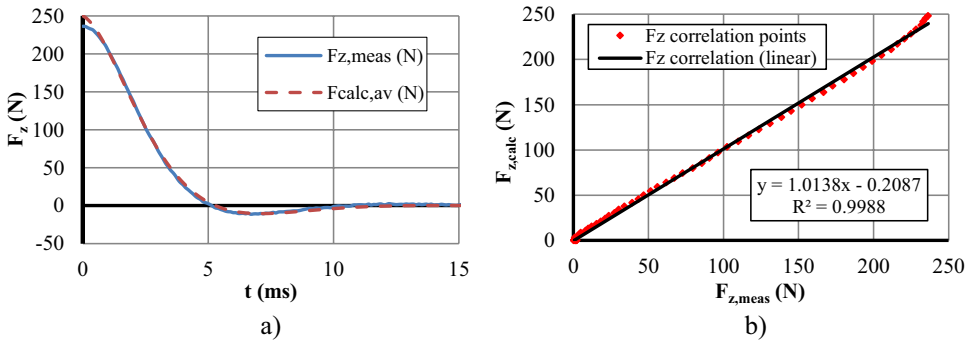

Fig. 20 Fit of the calculated F_{dec} values for symmetrical milling of X5CrNi18-10 steel to the average of the detected values (see Fig. 11). **a** The measured and calculated curves. **b** Correlation

reality, and on the other hand, the curves calculated from the decay data with the mapping shown in Figs. 15 and 16 also fit well with the measured data of the actual cutting. For milling, in the case of a chip thickness that can be considered uniform, formula (15) can be used to calculate the cutting force.

6 Energetic investigation and discussion

Based on the above, it can be concluded that from an energetic point of view, the cutting and the force measuring system can be considered as a single dynamic unit. A constant force effect, illustrated by the thick green line in Fig. 24, can be expected during the intermittent removal of a material section with a constant cross section and shape. On the other hand, the time-curve F_{cut} detected on the output side of the dynamometer only gradually, asymptotically approaches this actual, certainly constant value of F_{fact}. And when the material removal stops, when the actual cutting force is zero, the detected force data show a decaying curve marked F_{dec}, which asymptotically approaches zero in undulations. In the case of cutting and the measurement system connected to it, this can be interpreted as the actual force pulse F_{fact} appearing on the input side—using a mechanical analogy—binds energy that reduces the detectable signal on the output side during charging:

$$I(t_{cut}) = \int F(t)dt \cong \sum_{t0}^{tcut} F_{fact}(t)\Delta t \tag{23}$$

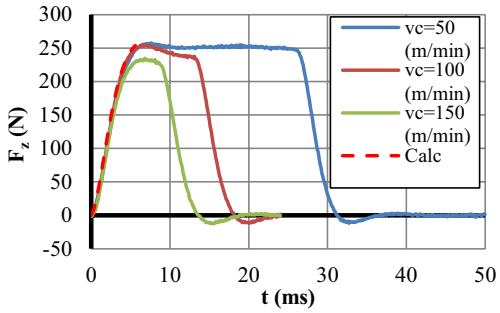

Fig. 21 Fit of calculated and measured force F_z during symmetrical milling of X5CrNi18-10 steel. $F_{z,cut}$ cutting force measured at $v_c = 50$, 100, and 150 m/min and the curve fitted to them (see Fig. 10)

This effect lasts until the end of chip removal, after which it no longer affects the value of the force F detected at the output. On the contrary, during decay, under the conditions of "air cutting," the pulse accumulated during the active measurement is degraded in the measuring system. According to the law of conservation of momentum, the sum of these two is zero.

In other words, during the decay, the pulse with which the system was saturated during cutting appears.

Consequently:

$$\sum_{t0}^{tcut} F_{cut}(t)\Delta t + \sum_{tcut}^{tcut+tdec} F_{dec}(t)\Delta t = \sum_{t0}^{tcut} F_{fact}\Delta t \tag{24}$$

With this condition $F_{fact} = \text{constant}$, the actual cutting force can be calculated from the force data detected during cutting and during decay:

$$F_{fact} \cong \left[N_{cut} + N_{dec}\right]^{-1} \left[\sum_{t0}^{tcut} F_{cut} + \sum_{tcut}^{tdec} F_{dec}\right] \tag{25}$$

As it can be seen, the duration t_{dec} of the summation is set indefinitely here during the decay. This only means that it is advisable to take into account as much of the detected decay data as possible. The experience so far is that satisfactory accuracy can be achieved if $t_{dec} = 5\tau$ is used from the decay using the usual method for electrical equipment. During this time, the decay can be considered complete from a technical point of view.

Table 3 The increase of the time constant τ during the decay

Phase	Time interval (ms)	Mean time (ms)	τ (ms)
Initial decay $t < t_{min1}$	0–4.84	2.42	2.87
$t_{min2} - t_{min1}$	4.84–17.90	11.37	8.76
$t_{max2} - t_{max1}$	11.45–24.13	17.79	13.56

Material: C45, $a_p{\cdot}f_z = 0.4{\cdot}0.8$ mm$_2$, $v_c = 200$ m/min, B/D = 58/80 mm/mm

In relation to Fig. 24, it can be stated graphically that according to the law of conservation of momentum, the entire area of the detected force curve, i.e., the area under the cutting and decaying section, must be equal to the product of $F_{fact} = \text{const.}$ actual force and cutting time t_{cut}. Since here, by definition, the technological data, thus the cutting force, is constant, this can be represented graphically with a rectangle. Its length is the cutting time t_{cut}, from this equality F_{fact} is obtained according to (16). Table 5 shows such test results.

Of course, this can only be stated if the change in the cross section of the removed material and the speed dependence of the forming resistance of the machined material can be ignored. Such measurement results are shown in Fig. 25, where the results of a series of measurements can be seen in which the thickness of the detached layer can be considered constant ($B/D = 21.4/80$ mm/mm, $a_p{\cdot}f_z = 0.4{\cdot}0.4$ mm^2). The figure was created according to the previously presented mirroring + offset method, the usability of which was confirmed by Fig. 12. However, it should be taken into account that not only the constant chip cross section is important here, but also, as already mentioned, that the cutting time exceeds the 5τ value. This depends on both the machined width B and the cutting speed. Figure 26 shows the curves of $F_y(t)$ values measured at a cutting speed in which the milled width was the same as in the test shown in Fig. 25,

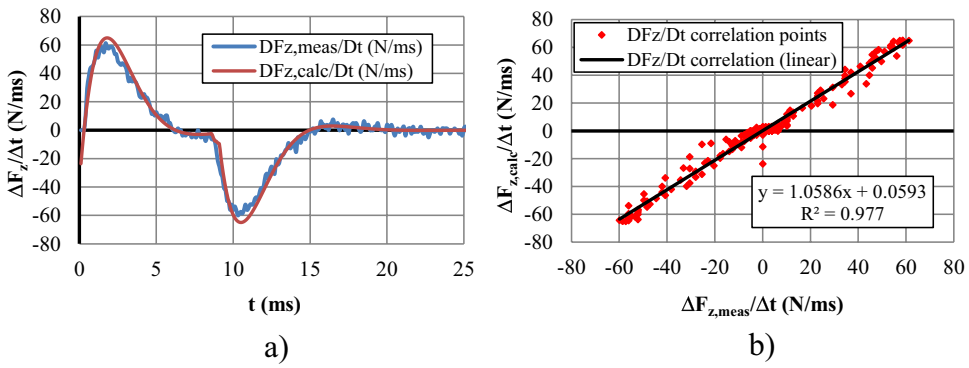

Fig. 22 Fit of the measured and calculated $\Delta F_z/\Delta t$ difference coefficients for symmetric milling (see Fig. 19)

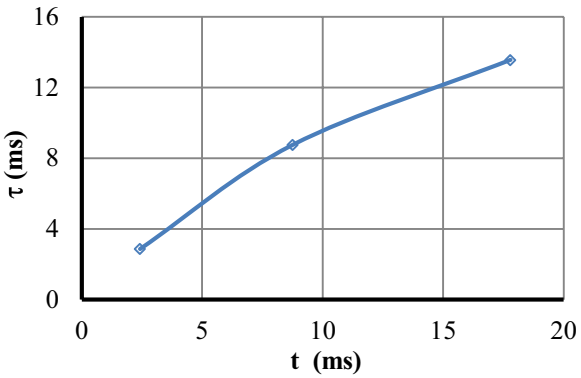

Fig. 23 The increase of time-constant τ during the decay (see Table 3)

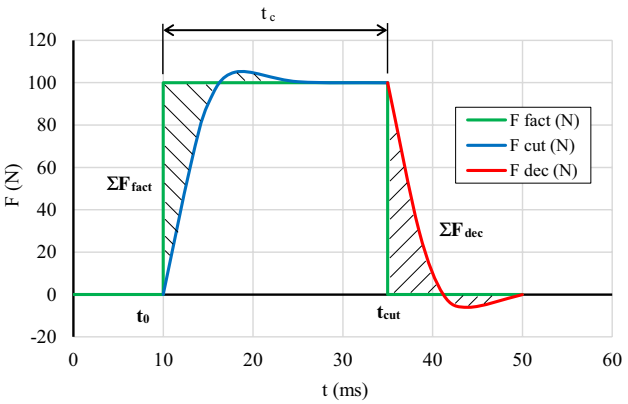

Fig. 24 The actual (Ffact) and detected (Fcut and Fdec) values of the cutting force when cutting a constant cross section

but the cutting speed was so high that the condition $t_{cut} > 5\tau$ was no longer met (X5CrNi18-10, $B/D = 21.4/80$ mm/mm, $a_p{\cdot}f_z = 0.4{\cdot}0.4$ mm^2).

However, there is still a possibility to approximate the cutting force in such cases. There is a part of the measurement series presented in Fig. 26 that is not affected by the length of the cutting time $t_{cut} < 5\tau$. These are the data series detected during decay. And since the measurements shown in Figs. 12 and 13 prove that the section of the $F_y(t)$ curve that was detected during cutting can essentially be produced by mirroring the curve section detected during decay. However, the $t_{cut} < 5\tau$ restriction no longer applies to the latter. The application of this is shown in Fig. 27, which was made with the data obtained from the measurement series presented in Fig. 26 at a cutting speed of $v_c = 250$ m/min. At this speed, the cutting time was $t_{cut} = 5.3$ ms, when $F_{y,cut} = 371$ N cutting force was detected. The decay curve was mirrored according to the method shown in Figs. 12 and 13 ($F_{y,dec,mirr}$) and moved back to time $t = 0$ ($F_{y,dec,mirr,move}$). The curve fluctuated asymptotically between 369 and 371 N, so $F_{y,fact} = 370$ N can be considered as the mean value of the actual cutting force.

Of course, it should be noted that the measured cutting force itself depends on many factors, such as the cutting speed. It is true that the data in Figs. 17 and 18 show that the force can be the same even in the case of a completely different chip formation process. However, it should be noted that this solution is a source of some uncertainty. It is known that the cutting force depends on the cutting speed regardless of the transient phenomenon. This can be traced back to the fact that the forming resistance of metals depends not only on the size of the deformation, but also on the speed of the deformation. It can be assumed, but so far it has not yet been discovered, whether the decrease or increase in the separated layer thickness affects the forming resistance, and therefore the cutting force, in a different way. The current investigation did not cover the study of these phenomena. The fact that a strong correlation of relationships could be established for the examined processes confirmed the assumption that these phenomena can be ignored in technological practice.

The result can be checked based on the law of conservation of energy. During the measurement, cutting took place for $t = 0$–5.3 ms, after which only the decay was detected by the measurement system. In order to realistically take the decay into account, the measured data must be used for a minimum period of 5τ. According to Table 4, the decay time constant for the used measurement system was $\tau = 2.27$ ms. Thus, $t = 25$ ms $> 5{\cdot}2.27$ ms, which meets the requirement $t_{cut} > 5\tau$. The total area under the curve detected was 19,529.1 N. In the measurement, taking into account the value of the time step $\Delta t = 0.1$ ms, 530 measurements

Table 4 Technical/statistical parameters of the electromechanical system used in cutting force measurements

	t_{n1} (ms)	Ω (ms^{-1})	τ (ms)
Average	5.04	0.53	2.87
Minimum	4.57	0.43	1.17
Maximum	5.4	0.62	2.75
Average deviation	0.2	0.03	0.35
Deviation	0.24	0.04	0.44

Table 5 The actual cutting force component F_z (N) in case of constant technological data

Material	$v_c = 50$ m/min	$v_c = 100$ m/min	$v_c = 150$ m/min
C45	172.3	181.7	188.7
X5CrNi18-10	252.6	244.2	223.5

Data: $a_p{\cdot}f_z = 0.4{\cdot}0.4$ mm^2, workpiece width $B = 21.4$ mm, tool in Chapter 2

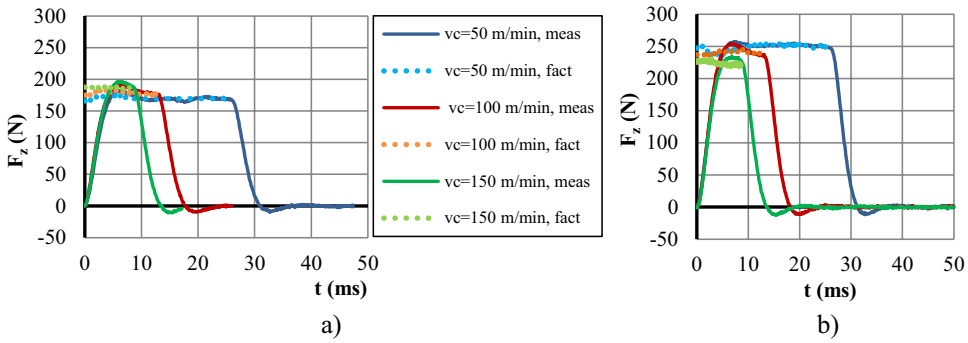

Fig. 25 The detected and actual cutting force in the case of a removed cross section that can be considered constant. **a** C45. **b** X5CrNi18-10

were made during cutting. As a result, the value of the actual cutting force, which was determined using this method, is $F_{y,fact} = \sum F_{y,det}/(t_{cut} + t_{det})\Delta t) = 19{,}529.1/53 = 368.5$ N. The difference is only $(370 - 368.5) \times 100/368.5 = 0.5\%$.

In order for the actual cutting force to be determined according to the law of conservation of momentum, it must be assumed that the actual cutting force can be described by an empirical function $F(t)$. In the case of Fig. 27, this was a $F(t) = \text{const.}$ function, which is only realized in a symmetric milling operation in which the change in the removed layer thickness is negligible. In such a case, only an empirical determination of a constant is necessary, for which the law of conservation of momentum is suitable. The situation is different, for example, with down- or up-milling, for which the known empirical formula is used:

$$F(t) \cong C f_z^{1-z} \sin^{1-z} \omega t \tag{26}$$

The usual interpretation of the specific cutting force $k = F/a_p f_z = k_{1.1}/h^z$, that is, in case of milling:

$$k_{1.1} = \frac{F}{a_p f_z^{1-z} \sin^{1-z} \omega t} \tag{27}$$

Equation (21) can be written as follows for milling according to the law of conservation of momentum:

$$\sum_{0}^{tcut} F_{cut}\Delta t + \sum_{tcut}^{tcut+\min 5\tau} F_{dec}\Delta t \cong k_{1.1} a_p f_z^{1-z} \sum_{0}^{tcut} (\sin^{1-z} \omega t)\Delta t \tag{28}$$

from which the constant of the specific cutting force can be calculated as follows:

$$k_{1.1} \cong \frac{\sum_0^{tcut} F_{cut} + \sum_{tcut}^{tcut+\min 5\tau} F_{dec}}{a_p f_z^{1-z} \sum_0^{tcut} \sin^{1-z} \omega t} \tag{29}$$

In this formula, the choice of the value of the z exponent requires special consideration. It is known that z is not only dependent on the material but is also affected by the thickness of the removed layer. A decreasing value of h corresponds to an increasing value of z. Here, in order to achieve the practical goal, i.e., to determine the real value of the cutting force, an approximate assumption must be used. Formula (26) helps with this, as it shows that the effect of the practical exponent z on $k_{1.1}$ is small. The results of the relevant calculations are shown in Fig. 28; according to the data of which, in the range $0.35 < z < 0.45$, the deviation of the value of $k_{1.1}$ from the mean value is 2% smaller (X5CrNi18-10, $a_p{\cdot}f_z = 0.4{\cdot}0.4$ mm^2, $v_c = 300$ m/min).

Down- and up-milling are typical cases of intermittent cutting with a highly variable cross section. For these, the cutting

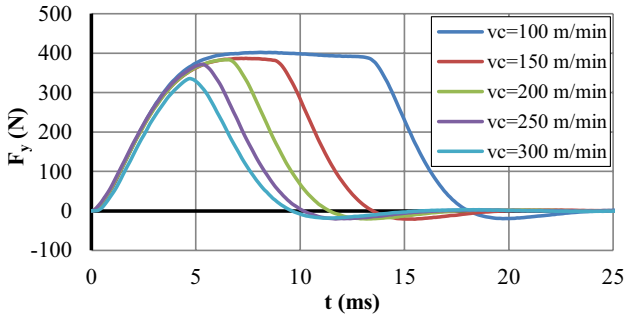

Fig. 26 Fy forces measured during symmetrical milling at different cutting speeds

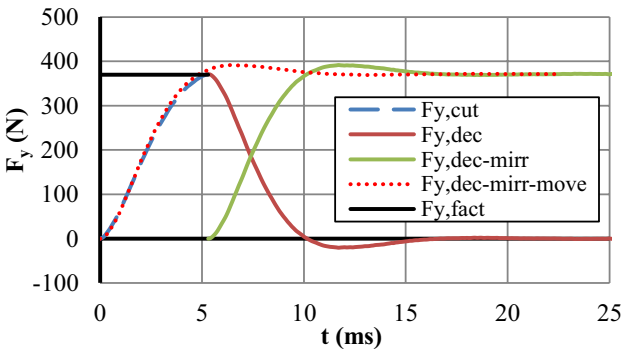

Fig. 27 Determination of the actual value of the cutting force $F_{y,fact}$ using the decay curve detected during the measurement at a cutting speed of $v_c = 250$ m/min. (see also Fig. 26)

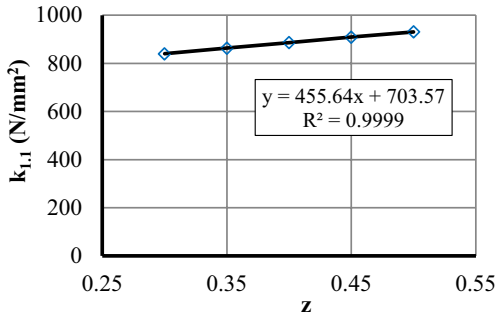

Fig. 28 The effect of the exponent z on the value of the specific cutting force $k_{1.1}$ calculated with formula (26) in down-milling

force and the mechanical power required for chip removal can only be calculated using the empirical formula (23) and Eq. (25). Using formula (23), the calculated cutting force at a given depth of cut a_p and feed rate f_z from the equation

$$\sum_{0}^{tcut+\min 5\tau} F_{meas}(t) \cong C_{calc} \sum_{0}^{tcut} \sin^{1-z} \omega t \tag{30}$$

is:

$$C_{calc} \cong \frac{\sum_{0}^{tcut+\min 5\tau} F_{meas}}{\sum_{0}^{tcut} \sin^{1-z} \omega t} \tag{31}$$

The application of this method is shown in Fig. 29, where it is striking how big the difference is between the curve of the cutting forces measured for up- and down-milling (C45, $a_p\, f_z = 0.4{\cdot}0.4$ mm^2, $v_c = 200$ m/min, $1 - z = 0.7$). This is especially evident in the section detected during the decay. According to Table 6, the momentum detected during decay—here indicated by the cutting force—is significantly smaller in down-milling than in up-milling, and this also applies to the data detected during active cutting. To calculate the actual cutting force, the exponent z of the basic formula (23) can only be given an estimated value, which can be considered as the specific average of the entire chip removal.

Table 6 Area calculations under the curves shown in Fig. 29

Milling type	$\sum F_{z,meas}$ (N)	$\sum F_{z,dec}$ (N)	C_{calc} (N)	$\sum F_{z,calc}$ (N)
Up	4181.0	561.5	571.2	4181.0
Down	3888.6	204.4	542.0	3888.6

(C45, $a_p{\cdot}f_z = 0.4{\cdot}0.4$ mm^2, $v = 200$ m/min, $1 - z = 0.7$)

The applicability of formula (23) may also raise the question of whether there is an effect of the operation being performed with decreasing or increasing cross section. This has the consequence that the two technological versions also differ in that the deformation and thus the change in the deformation speed are different. As a result, the forming resistance (shear stress) and thus the cutting force are different. This also explains why the cutting speed affects the specific cutting force. It provides information on how to evaluate the two methods of milling in terms of energy consumption and the load on the structure. Figure 30 shows that in terms of the magnitude of the generated cutting force, down-milling is more favorable (C45, $a_p{\cdot}f_z = 0.4{\cdot}0.4$ mm^2, $v_c = 200$ m/min, $1 - z = 0.7$). It is also obvious that the difference between the two milling methods from an energetic point of view is practically independent of the magnitude of the exponent z; it is constant. Figures 28 and 30 together show that formula (23) and the relationships derived from it can be used in practical calculations.

The energy requirement for chip removal can be calculated using formula (22) derived from the law of conservation of momentum. On the basis of the comparative measurement, the results of which are shown in Fig. 29, in the case of the specific technology, the energy need for down, up, and symmetrical milling can be calculated and compared. The information required for the calculation is provided by the detected data. These are summarized in Table 7. The differences cannot be considered significant. It is a fact that the difference between the energy requirement established for down- and up-milling is small.

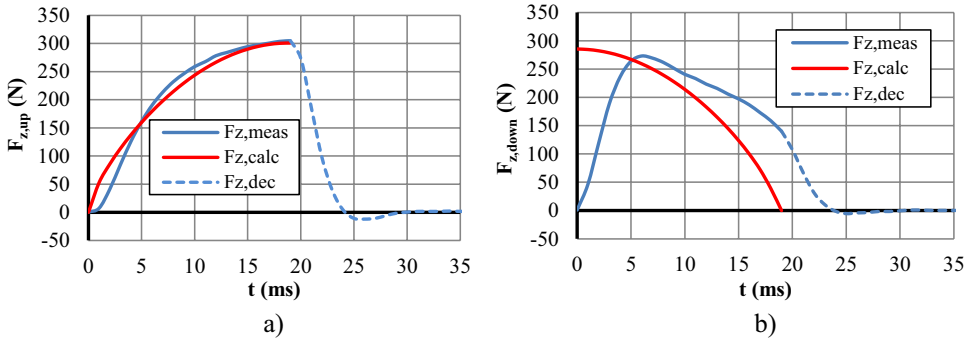

Fig. 29 The detected force component F_z for a up-milling and b down-milling

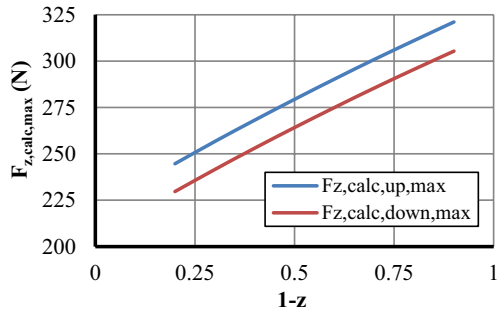

Fig. 30 The effect of the exponent of formula (23) on the calculated cutting force $F_{z,calc}$

Although there is no doubt that the deformation process of the material is certainly not exactly the same in the two cases, a deep plasticity theory analysis would be necessary to judge the difference. Thus, in the final result, it can be concluded that the difference in energy consumption for the two milling versions examined can be ignored from the point of view of practice. The lower energy requirement for symmetric milling can be traced back to the fact that the average chip thickness was greater, and the average specific cutting force was lower than in the other two versions. All of this can be summed up in the fact that the method derived from the mathematical model is suitable for calculating the energy requirement of cutting.

According to previous investigations, during milling, a transient ramp-up phenomenon is experienced at the beginning of the time-curve of the detected cutting force. With further force measurements, it was possible to establish that

Table 7 Calculation of the energy requirement of chip removal for different milling versions

Milling version	Down	Symm	Up
B (mm)	40	58	40
V (mm^3)	1.6	2.32	1.6
$\varphi 0$ (°)	90.7	43	1.4
t_0 (ms)	19	9	0.3
φ_{cut} (°)	191.4	138.5	91.4
t_{cut} (ms)	38	29	19.3
t_c (ms)	19	20	19
$\sum_{to}^{tcut+tdec} F_{meas}$ (N)	4108.5	5659	4748.4
$\sum_{to}^{tcut} F_{meas}$ (N)	4034.7	5213	4187
$\sum_{tcut}^{tcut+tdec} F_{meas,cut}(N)$	73.6	446	561.4
L (J)	13.7	19	14.2
$Q=L/V$ (J/mm^3)	8.6	8.2	8.9

Geometric and kinematic conditions: see Fig. 2

the measurement technique together with the technological process forms a dynamic mechanical-electronic system. This also affects the detected signals, which must be taken into account when measuring short cutting sections. The operation of the measuring system is therefore not limited to the time of chip removal, because due to the decay, a non-zero signal is also detected during the "air cutting" after material removal.

The measurements consistently showed that two phases can be distinguished during the decay: the initial, rapid decrease of the detected force data and the subsequent wave, the amplitude of which decreases further. The zero points of the undulation and the wavelength are practically the same even in the case of very different feed rates. The decay dynamics are therefore the same. This can only be traced back to the dynamic characteristics of the electromechanical measuring system. It could be established that regardless of the technological data (feed and cutting speed) and the quality of the tested steel, the main parameters of the detected decay and the subsequent undulation—the zero locations and the locations of the force extremes, i.e., the wavelength—are almost identical on the time scale t.

It has been proven that the transient phenomenon observed at the beginning of the cutting phase is related to the dynamics of decay. The decay curve can be mirrored and moved onto the rising section of the cutting. The correlation between the curve sections detected at the start of cutting and at the decay is close. In the case of a constant thickness of the removed layer (this was practically the case with symmetric milling), the force curve measured during the initial, transient phase of the cutting was a direct reflection of the curve detected during decay. The characteristic of X5CrNi18-10 steel chips is the well-known lamellar structure, in which two very differently deformed material layers alternate periodically. In this investigation, a sampling frequency of 100 kHz was also used, but the transient processes at the detected cutting force were the same as those that could be registered when milling C45 carbon steel.

A mathematical model was developed for the theoretical study of the dynamic behavior of the force measuring system. For this, the theory of a series-connected RCL circuit was used.

When cutting variable layer thicknesses, such as down- and up-milling, additional information is required to determine the actual cutting force. In the case of the most frequently used Kienzle formula, this can be solved by an approximate determination of the exponent z. By using this value, it became possible to empirically determine the cutting force $F_{fact}(t)$, which varies according to the technology. The determination of the energy requirement is possible using the law of conservation of momentum applied to the mathematical model.

The presented results can obviously only be considered as representative results for the used measurement system; we did not have the opportunity to compare the obtained data with decay phenomena experienced in other force measurement systems. However, the revealed relationships can probably also be used for other force measuring systems, taking into account the characteristics of the actual measuring system.

As a further direction of development, the extension of the model obtained for one insert to machining with several cutting edges, the addition of handling the superimposition of individual force diagrams can be considered.

Another potential direction for future studies may be a more precise determination of the actual cutting force in the initial stage of the milling operation: a mathematical and experimental analysis of the changing cutting force and the dynamics of the measuring system as a result of the nature of the milling technology.

Abbreviations Markings

a_p (mm): Depth of cut; f_z (mm/rev): Feed per edge; $i(t)$ (mA): Amperage in Eq. (1); k (N/mm^2): Specific cutting force; $k_{1.1}$ (N/mm): Constant of the specific cutting force; r_ε: Nose radius; t (ms): Time; t_c (ms): Duration of the cutting phase; t_{cut} (ms): The end time of the cutting phase; $t_{n,i}$ (ms): The i-th zero-place of the decay ($i=1, 2, 3$); $t_{min,i}$ (ms): At decay, the i-th minimum position of the wave ($i=1, 2$); t_{cikl} (ms): Cycle time of the wave at decay; $u(t)$ (mV): Voltage in Eq. (1).; v_c (m/min): Cutting speed; z: Exponent of the specific cutting force formula; B (mm): Specimen width; C: Constant in formula (23); C (F): Capacity; C_{calc}: Calculated constant in formulas (27) and (28); C_F (N): Constant, the multiplier of the decay formula (13); C_{part}: Constant in formula (2); C_Ω: Ripple constant in formula (14); D (mm): Cutter diameter; F_c, F_f, F_p (N): Main cutting force, feed force, passive force; F_x, F_y, $F_z=F_p$ (N): X, y, z components of the cutting force; F_{cut} (N): Detected cutting force at time $t=t_{cut}$; F_{fact} (N): Actual cutting force; F_{dec} (N): Apparent force detected at decay; F_{meas} (N): Measured cutting force; I (Ns): Momentum (impulse); I_{fact} (Ns): Actual impulse; I_{meas} (Ns): Detected impulse; L (H): Inductance; L (J): Mechanical work carried out; N: Number/pieces; Q (J/mm^3): Specific energy; R (Ω): Electrical resistance; R^2: Squared correlation coefficient; S_{cut}: Cutting stage; $S_{dec,i}$: Initial stage of decay; $S_{dec,w}$: Undulating phase of decay; α (°): Clearance angle of cutting insert; γ (°): Rake angle of the cutting insert; κ_r (°): Principal cutting edge angle; κ_r' (°): Auxiliary cutting angle; φ (°): Angular rotation of the cutter; φ_{cut} (°): The angular position of the cutter at the end of the cutting section; τ (ms): Time constant of the decay; ω (rad/ms): Circular frequency of the cutter body; ω_0 (rad/ms): Self-frequency of the measuring system; Φ (rad): Phase angle, the angular position of the decay; Ω (rad/ms): Requency of the self-wave after the fast decay

Indexes

calc: Calculated; cut: Cut; dec: Decay; down: In case of down-milling; fact: Factual; meas: Measured; mirr: Mirrored; move: Moved; symm: In case of symmetric milling; up: In case of up-milling

Acknowledgements The research was partly supported by the research project K 132430 (Transient deformation, and thermal and tribological processes at fine machining of hard metal surfaces) provided by the National Research, Development and Innovation Office in Hungary.

Author contribution All authors contributed to the study conception and design. Material preparation, data collection, and analysis were performed by Z. Pálmai, T. Makkai, and C. Felhő. The first draft of the manuscript was written by Z. Pálmai and J. Kundrák, and all authors commented on previous versions of the manuscript. All authors read and approved the final manuscript.

Funding Open access funding provided by University of Miskolc. The research was partly supported by the research project K 132430 (Transient deformation, thermal and tribological processes at fine machining of hard metal surfaces) provided by the National Research, Development and Innovation Office in Hungary.

Declarations

Competing interests The authors declare no competing interests.

References

1. Finnie (1956) Review of the metal-cutting analyses of the past hundred years. Mech Eng 715–721.
2. Bayard O (2000) Investigation of the verification techniques for modelling turning processes. Royal Institute of Technology, Dept. Material Processing, Production Engineering, Stockholm
3. Ghani MU, Abukhshim NA, Sheikh MA (2008) An investigation of heat partition and tool wear in hard turning of H13 tool steel with CBN cutting tools. Int J Adv Manuf Technol 39:874–888
4. Suresh R, Basavarajappa GL (2012) Samuel, Predictive modelling of cutting forces and tool wear in hard turning using response surface methodology. Procedia Engineering 38:73–81

5. Li Z, Wang G, He G (2017) Milling tool wear state recognition based on partitioning around medoids (PAM) clustering. Int J Adv Manuf Technol 88:1203–1213
6. Chuangwen X, Jianming D, Yuzhen C, Huaiyuan L, Zhicheng S, Jing X (2018) The relationship between cutting parameters, tool wear, cutting force and vibration. Adv Mech Eng 10(1):1–14
7. Navarro-Devia JH, Chen Y, Dao DV, Li H (2023) Chatter detection in milling processes—a review on signal processing and condition classification. Intl J Adv Manuf Technol 125:3943–3980
8. Tomicek J, Molotovnik A (2016) Influence of cutting conditions on profile milling of INCONEL 738LC alloy. Manuf Technol 16(2):461–467
9. Pan Z, Feng Y, Lu YT et al (2017) Force modeling of Inconel 718 laser-assisted end milling under recrystallization effects. Int J Adv Manuf Technol 92:2965–2974. https://doi.org/10.1007/s00170-017-0379-x
10. Song Chunlei (2023) A novel high-order discretization method for the milling stability prediction considering the differential of directional cutting coefficient and vibration velocities. Intl J Adv Manuf Technol 125:5221–5231
11. Cekic A, Begic-Hajdarevic D, Kulenovic M (2013) Effect of the cutting parameters on cutting forces in high speed face milling. Technicki Vjesnik 20(5):775–780
12. Biró I, Czampa M, Szalai T (2015) Experimental model for the main cutting force in face milling of a high strength structural steel. Periodica Polytechnica Mech Eng 59(1):16–22
13. Salomon C (1929) Schnittdruck und Schneidtemperature Erscheinungen an der Werkzeugschneide. Die Werkzeugmaschine, Zeitschrift für Metallbearbeitung und Maschinenbau, 33 Jahrg. Heft 23:477–496
14. König O, Victor H (1957) Spezifische Schnittkrafte bei der Metallbearbeitung Werkstattstechnik und Maschinenbau 47:22–25
15. Turkovich BF (1967) Dislocations theory of share stress and strain rate in metal cutting. Advanced in Machine Tool Design and Research, Proceedings of the 8th International CIRP Production Engineering Research Conference, University of Manchester, Institute of Science and Technology, pp. 507–526.
16. Black JT (1971) On the fundamental mechanism of large strain plastic deformation, electron microscopy of metal cutting chips. J Eng Ind 93:507–526
17. Black JT (1972) Shear front-lamella structure in large strain plastic deformation processes. J Eng Ind 94:307–316
18. Black JT (1979) Flow stress model in metal cutting. J Eng Indust 101:403–415
19. Ramalingam S, Black JT (1973) An electronmicroscopy study of chip formation. Metallurg Trans 4:1103–1112
20. Qing-Jie Li Ju, Li Z-W, Ma E (2016) Strongly correlated breeding of high-speed dislocations. Acta Mater 119:559–241
21. Li QJ, Li J, ZW, Ma E, (2016) Strongly correlated breeding of high-speed dislocation. Acta Mater 119:229–241
22. Melcote SN, Fernandez-Zelaia LR (2015) A physically based constitutive model for simulation of segmented chip formation in orthogonal cutting of commercially pure titanium. CIRP Ann 64:65–68
23. Rodriguez JM, Jonsen P, Svoboda A (2017) Dislocation density based material model applied in PFEM-simulation of metal cutting. Procedia CIRP 58(2017):193–197
24. Xu X, Zhang J, Outeiro J, Xu B, Zhao W (2020) Multiscale simulation of grain refinement induced by dynamic recrystallization of Ti6Al4V alloy during high speed machining. J Mater Process Technol 286:116834
25. Bai J, Tong Z (2021) A novel multiscale material plasticity simulation model for high-performance cutting AISI 4140 steel. Intl J Adv Manuf Technol 116:3891–3904
26. Pálmai Z, Kundrák J, Makkai T (2019) The transient changing of forces in interrupted milling. Intl J Adv Manuf Technol 104:3757–3801